Invited Paper

# Functional Interactions in Hierarchically Organized Neural Networks Studied with Spatiotemporal Firing Patterns and Phase-Coupling Frequencies

Stephen Perrig[1], Javier Iglesias[2, 3], Vladislav Shaposhnyk[3], Olga Chibirova[3],
Pierre Dutoit[3], Jérémie Cabessa[3], Katerina Espa-Cervena[1], Laurent Pelletier[3],
François Berger[3], and Alessandro E.P. Villa[1, 3, 4]

[1]*Sleep Research Laboratory, Department of Psychiatry, Hôpitaux Universitaires de Genève*
*Chêne-Bourg, Switzerland*
[2]*Departament de Física i Enginyeria Nuclear, Universitat Politècnica de Catalunya, Terrassa, Spain*
[3]*Grenoble Institut des Neurosciences (GIN), INSERM, UMR_S 836, NeuroHeuristic Research Group*
*Université Joseph Fourier, Grenoble, France*
*and*
[4]*Neuroheuristic Research Group, Information Systems Department ISI, University of Lausanne*
*Switzerland*

## Abstract

A scalable hardware/software hybrid module –called *Ubidule*– endowed with bio-inspired ontogenetic and epigenetic features is configured to run a neural networks simulation with developmental and evolvable capabilities. We simulated the activity of hierarchically organized spiking neural networks characterized by an initial developmental phase featuring cell death followed by spike timing dependent synaptic plasticity in presence of background noise. An upstream 'sensory' network received a spatiotemporally organized external input and downstream networks were activated only *via* the upstream network. Precise firing sequences, formed by recurrent patterns of spikes intervals above chance levels, were observed in all recording conditions, thus suggesting the build-up of a connectivity able to sustain temporal information processing. The activity of a *Ubinet* –a network of *Ubidules*– is analyzed by means of virtual electrodes that recorded neural signals similar to EEG. The analysis of these signals was compared with a small set of human recordings and revealed common patterns of shift in quadratic phase coupling. The results suggest some interpretations of changes and plasticity of functional interactions between cortical areas driven by external stimuli and by learning/cognitive paradigms.

Key Words: apoptosis, spike timing dependent plasticity, synaptic pruning, preferred firing sequence, insomnia, EEG

## Introduction

The embryonic nervous system is initially driven by genetic programs that control neural stem cell proliferation, differentiation, and migration through the actions of a limited set of trophic factors and guidance cues (24, 35). The outcome of this phase is a pattern of neuronal connectivity characterized by a

large amount of diffusely distributed branches and synapses. The rapid rate of synaptogenesis begins a few weeks after the end of neurogenesis and completion of neuronal migration. After a relatively short period of stable synaptic density, a pruning process begins: synapses are constantly removed, yielding a marked decrease in synaptic density (25). For the human brain, the peak level of synaptic density in childhood is 150 to 200% compared to adult levels, depending on the brain region (9, 19). This suggests a gradient-like organization during early corticogenesis (13, 39) that is likely to be related to cortical patterns of gene expressions (51). The refinement of the nervous system is due to apoptosis –genetically programmed cell death– and selective axon pruning (25, 27, 28).

It is rationale to suppose that the final outcome of complex connectivity patterns is the result of the pruning of only a selected subset of the connections initially established by a neuron. Overproduction of a critical mass of synapses in each cortical area may be essential for their parallel emergence through competitive interactions between extrinsic afferent projections (8) as suggested by competing projections of the two eyes during the formation of visual centers (18). Furthermore, background activity and selected patterns of afferent activity are likely to shape deeply the emergent circuit wiring (30, 43).

Synapses can change their strength in response to the activity of both pre-, and post-synaptic cells following spike timing dependent plasticity (STDP) rules (40). This property is assumed to be associated with learning, synapse formation, and pruning. The strength of the synapses may vary between discrete mechanistic states (31), rather than by adjusting their efficacy along a continuum, that allows an efficient modeling of the mechanism (46). Certain pathways through the network may be favored by preferred synaptic interactions between the neural elements as a consequence of developmental and learning processes (6). In cell assemblies interconnected in this way some ordered and precise –in the order of few *ms*– interspike interval relationships, referred to as "spatio-temporal firing patterns" or "precise firing sequences", may recur within spike trains of individual neurons and across spike trains recorded from different neurons (1). If functional correlates of spatio-temporal neural coding exist, one would expect that whenever the same information is presented, the same temporal pattern of firing would be observed (47, 48).

At mesoscopic level, the recording of brain activity by means of electroencephalography (EEG), electrocorticography (ECoG) and local field potentials (LFP) collects the signals generated by multiple cell assemblies. The neurophysiological processes underlying those signals are determined by highly non-

linear dynamic systems (34). The functional interactions between brain areas that are simultaneously sampled by these signals can be better investigated by third order polyspectral analysis that retain phase relationships (7). This analysis is a non-linear method of signal processing that quantifies the degree of phase coupling and was applied to EEG by pioneers as early as the 1970s (11). Phase coupling frequencies can be interpreted as frequencies of resonance of standing waves whose wavelength is associated to the average distance between interacting cell assemblies (49, 50).

In the present study we simulated the activity of interconnected neural networks undergoing neural developmental phases. The implementation of such complex models requires high performance of the simulation that can be achieved thanks to a powerful hardware platform, its bio-inspired capabilities, its dynamical topology, and generic flexibility of artificial neuronal models. We briefly present the layout of a hybrid platform for the neural system simulator as a powerful and innovative simulation tool for neural simulation and modeling. The outcome is the implementation of each neural network into a *Ubidule* and a network of *Ubidules* as a *Ubinet*.

At first, a couple of networks are organized such that selected units assumed to correspond to the output layer of an upstream network project to the input layer of a downstream network. The upstream network is the only one receiving an external input activity and may be viewed as a "sensory cortical area" receiving afferences from the ascending sensory pathway. In this framework the downstream network may correspond to a "secondary cortical area". The output spike trains of the networks were scanned to detect precise firing sequences, whose structure and dynamics were analyzed and compared with the results obtained for the single simulated networks in presence and in absence of stimuli (20). The emergence of functional connectivity driven by neural development, cell and synaptic pruning, and selective external stimuli was further assessed in a *Ubinet* by recording Electrochipograms (EChG) which are analog signals similar to EEG generated by virtual electrodes located into each *Ubidule*.

We analyzed the EChG mainly by higher-order spectral analyses in order to reveal quadratic phase coupling using the same techniques applied for real brain recordings. The experimental setup was aimed to describe what happened prior to, at the beginning, towards the end, and after repeating an external input at fixed frequency. The rationale is that the spike timing dependent plasticity embedded in the neural network models would drive the build-up of auto-associative network links, within each *Ubidule*, such to generate an areal activity, detected by EChG, that

would reflect the changes in the corresponding functional connectivity. This experiment is compared to a small set of recordings performed in patients suffering of primary insomnia whose EEG recordings were analyzed during several sleep phases, before and after a clinical treatment.

## Large Scale Neural Network Simulations

### Features of the Neural Network

In this study we extend to two (and more) interconnected networks the framework for artificial neural network simulation that was previously developed for implementation of several features of brain maturation (22, 23). Each network is a 2D lattice of $100 \times 100$ units –80% of excitatory units and 20% of inhibitory units– uniformly distributed over the network according to a space-filling quasi-random Sobol distribution (38). The probability that, within each network, a unit be connected to another one followed a Gaussian density function with different parameters for excitatory and inhibitory units (21). All units were simulated by leaky integrateand-fire neuromimes. The spike trains of neuromimes were recorded and searched for precise firing sequences (PFS).

Background activity was used to simulate the effect of afferences that were not explicitly simulated within a network. To this end we assumed that all units received the same number of external inputs and that all of these were excitatory. Both apoptosis and synaptic pruning were taken into account in presence of a background noise (22). Apoptosis was active only at the begin of each simulation run; in this study apoptosis was active during the initial 700 time units. Synaptic plasticity was active from the end of apoptosis until the end of simulation. It is assumed *a priori* that modifiable synapses were characterized by activation levels with 4 attractor states (21). The activation level could jump from one state to another according to the pre- and postsynaptic spike ordering following a STDP rule. Synaptic pruning occured when the activation level of a synapse reached a value of zero. Besides cell death and axonal pruning of dead cells provoked by apoptosis, the units whose all synaptic connections were characterized by a zero level of activation were definitely eliminated from the network. In each network two sets of 400 excitatory units (*i.e.*, 800 units overall) were randomly selected among the 8,000 excitatory units. These units corresponded to the "input layer" of the network, meaning that in addition to sending and receiving connections from the other units of both types (excitatory and inhibitory) within the network they received an external input.

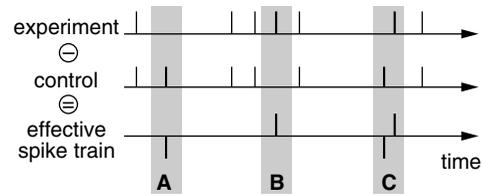### Preferred Firing Sequences



Fig. 1. The experimental conditions alter the spike timing of the units with respect to a control condition. An effective spike train is computed by subtracting the spikes recorded in the control simulation (including the background activity) to the spikes recorded in the experiment in order to quantify these changes. Three types of differences can be accounted for (A) deleted episodes relative to the control condition; (B) inserted episodes relative to the control condition; and (C) drifted (anticipated or delayed) episodes which result in both a deleted and an inserted episode in the effective spike train.

For each network we recorded separately the spike trains due to the effects of background noise only. These recordings corresponded to a "control condition" necessary to evaluate the "effective spike trains" (Fig. 1) that represent the genuine activity due to network dynamics (17).

All Preferred Firing Sequences were searched in the effective spike trains. PFS were defined as sequences of intervals with high temporal precision between at least 3 spikes (triplets) of the same or different units that recurred at levels above those expected by chance by means of the "pattern grouping algorithm" (PGA) (Fig. 2). PFS can be formed by spikes generated by one unit only. In this case PFS are referred to as 'single-unit patterns'. PFS that include spikes generated by different units are referred to as 'multi-unit patterns'. For the present study PGA (44) was set to find patterns formed by three (triplets) or four spikes (quadruplets), with a significance level $p = 0.10$, provided the entire pattern did not last more than 800 *ms* and was repeated with a jitter accuracy of $\pm 5$ *ms*.

### Recording Conditions

The detailed spike train activity was studied in paired *Ubidules* configuration. In the upstream network a subset of excitatory units not belonging to the input layer was selected as "output layer". The output layer was formed by all units maintaining at least five active excitatory input connections from within the network after a simulation run lasting 100.000 *ms* with time resolution of 1 *ms*. This duration was fixed arbitrarily because the networks generally stabilized or died by this time. The amount of units belonging to the output layer was in the range 100-150, depending
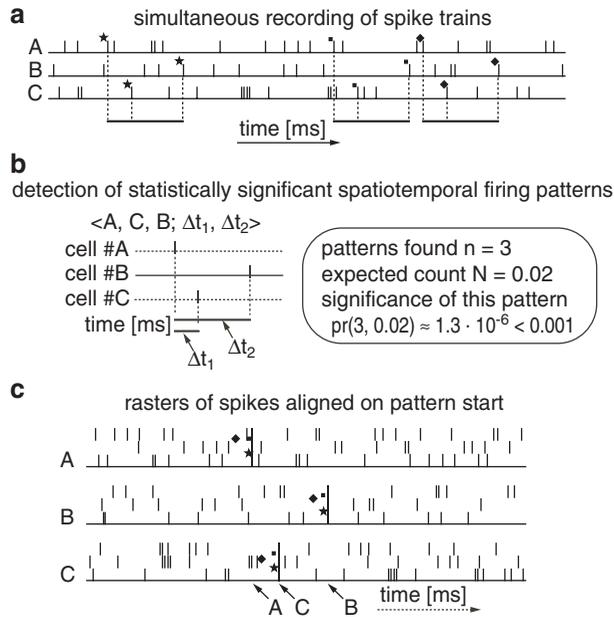
Fig. 2. Outline of the general procedure followed by pattern detection algorithms. (**a**): Analysis of a set of simultaneously recorded spike trains. Three cells, labeled A, B, and C, participate to a patterned activity. Three occurrences of a precise pattern are detected. Each occurrence of the pattern has been labeled by a specific marker in order to help the reader to identify the corresponding spikes. (**b**): Estimation of the statistical significance of the detected pattern. (**c**): Display of pattern occurrences as a raster plot aligned on the pattern start.
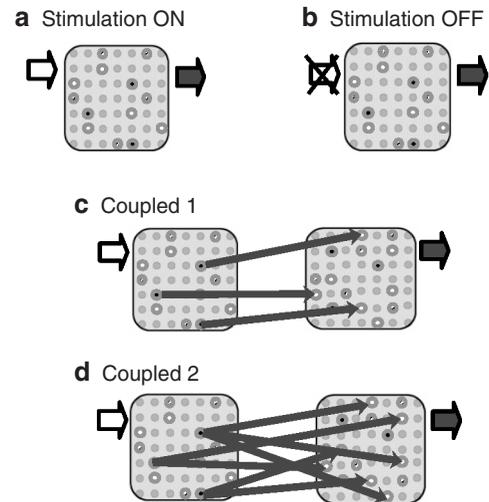


Fig. 3. Schematic diagram of the four recording conditions. In panels (a) and (b) the networks are isolated. In panels (c) and (d) the networks are coupled. The upstream network is on the left hand side and the downstream network on the right hand side.

on the random number generator initialization. Notice that the connections between the output layer of the upstream network and the input layer of the downstream network are synaptic connections with the activation level invariant throughout the simulation and with synaptic strengths identical to the afferent sensory projections.

We distinguish four recording conditions (Fig. 3):

*'stim OFF'*: The activity of a single network was recorded in the absence of any external input and in presence of the background noise only. The effective spike trains represented the net effect of internal network dynamics shaped by spontaneous synaptic pruning.

*'stim ON'*: The activity of the upstream network was recorded in presence of an external input corresponding to a spatiotemporal pattern of activity (22).

*'coupled 1'*: The activity of the downstream network was recorded in presence of an external input fed to the upstream network. The pattern of connectivity between the two networks was such that each unit of the upstream output layer was connected to only one unit of the downstream input layer, randomly selected among the predefined 800 input units.

*'coupled 2'*: The activity of the downstream network was recorded in presence of an external input fed to the upstream network. The pattern of connectivity between the two networks was such that the upstream output layer was characterized by divergent projections onto the downstream input layer. Each of the 800 units of the downstream input layer were receiving a projection from one unit of the upstream output layer.

## The Ubinet

*Hybrid System Implementation*

The *Ubidule* is a custom reconfigurable electronic device allowing an implementation of several bioinspired mechanisms such as growth, learning, and neural processing (41). The common *Ubidule* platform is an hybrid system with two main characteristics. The first is an XScale-class processor that manages the software components of the system, such as communications with other *Ubidules*, monitoring, but also phylogenetic processes. This processor is equipped with an open hardware subsystem which allows connecting any sort of USB device (sensors, actuators, Wifi/Bluetooth dongles, mass storage, *etc.*).

The processor runs an embedded Linux operating system which facilitates *Ubidule* programming and management while ensuring portability at the same time. The second characteristic is a full custom reconfigurable electronic device named *Ubichip* which can be configured either in native mode (FPGA like) or in multiprocessor mode.

Both hardware and software platforms are based upon modular architecture according to the classical evolutionary scheme along three main axis, that are Phylogenesis, Ontogenesis, and Epigenesis. *Phylogenesis* deals with the evolution of the species. Evolution is meant to gear species towards a better adaptation of individuals to their environment by means of mutation of the basic instruction set (the *genome*). Genetic algorithms are inspired from this very principle of life by selecting the individuals according to some fitness function. *Ontogenesis* describes the origin and the development of an organism during its early stages. Biological processes like cell proliferation, cell differentiation, healing and fault tolerance are qualified of ontogenetic. *Epigenesis* refers to adaptation, learning and plasticity unrelated to the specific DNA sequence of an organism. Learning performed by artificial neural networks is a process limited to an individual lifetime and is qualified of epigenetic.

The similar modular structure offers interoperability among the hardware and the software parts of the system and simplifies the usage of bio-inspired features of the hardware. The neural system simulator consists of multiple computational modules, each one corresponding to a neural network, exchanging their neural activity and/or receiving input data from hardware sensors (camera, photodiode, radars, *etc*.) and/ or providing output to hardware actuators (motor, diode array, *etc*.). The characteristics of the implementation naturally geared the modeling framework towards agent oriented programming. An evaluation of the available platforms of this kind led us to select JADE (3) for the development and runtime execution of peer-to-peer applications which are based on the agent oriented paradigm.

The phylogenetic evolutionary level of the application (P-agent) carries the genetic algorithm associated to the computational neurogenetic modeling (4). Notice that many neuronal applications without P-agent may be bound to one application with P-agent. The P-agent generates the genomes for the application set and translates genomes to the appropriate ontogenetic O-agents for further initialization and generation of the Eagents. The fitness function, also associated to the P-agent, collects information about system behavior and selects the "best" genomes to produce the next generation of agents replacing the "dead" ones. In the current implementation no specific
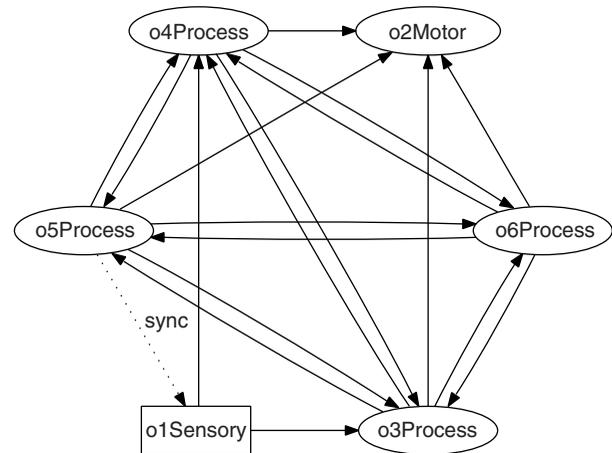


Fig. 4. The *Ubinet* circuit used in all simulations. Solid arrows depict connections and directions of information flow between the *Ubidules*. The dotted arrow describes an auxiliary technical synchronization connection ensuring a common *Ubinet* time flow.

task was required and the fitness function was merely reduced to the survival of the *Ubinet*. The survival was fulfilled if *(i)* the activity within the networks modules was maintained despite the cell and synaptic pruning driven by spike timing dependent plasticity; *(ii)* the *Ubinet* achieved foraging (2) and mating activities (10). An agent "life-time" is implemented, mimicking biological principle of natural selection, preserving the genomic properties associated to the best fitted "individuals". The ontogenetic level of the application (O-agent) is devoted to decoding the genome (provided by the P-agent), managing genome mutations, configuring the neural network elements (cell types with their specific dynamics) and all other auxiliary setup steps necessary to ensure the integrity of the software/hardware platform.

*Electrochipograms*

Our circuit topology remained fixed during all simulations and the *Ubidules* were characterized by their role in the network, *i.e.*, *sensory*, *processing*, or *motor* (Fig. 4). In our network, the *o1Sensory Ubidule* has a pure sensory role. *Ubidules* labeled *o3Process*, *o4Process*, *o5Process*, *o6Process* have a pure information processing role and are characterized by having neither external inputs nor afferences from the motor *Ubidule*. They are all reciprocally interconnected and send efferent projections to *o2Motor*.

Our design of the bio-inspired artificial neural networks allowed us to implement realistic virtual electrodes to record neuro-mimetic signals, called *Electrochipograms* (EChG), characterized by dynamics and features similar to those recorded in living brain structures.

In our implementation the virtual electrode measures the potentials over a certain 'area' of the 2D lattice neuronal network according to an appropriate weighted sum (42). The main parameters of the electode are its position over the neural network and its sensibility function. The position $C = (x, y)$ is defined by the two dimensional coordinates of the centre of the electrode on 2D square lattice of the neural network. The tip of the virtual electrode was located in the middle of the 2D lattice of each *Ubidule* neural network.

The sensibility function depends only on the distance between a given point of the lattice and the centre of the electrode field. According to this model, all neurons located at the same distance from the center of the electrode field make an equivalent contribution to the final electrode output and thus form an equi-potential layer $L$. Let us denote $R$ the sensibility radius of the electrode corresponding to the total number of the equipotential layers contributing to the signal recorded by the electrode. The monopolar signal recorded by the radial electrode is calculated such that $E_{monop}(t) = \sum_{r=1}^{R} \varphi(r) \sum_{\forall i \in L(r)} \Psi_i(t)$, where $\varphi(r)$ is a given sensibility function of the electrode, $L(r)$ is the set of all neurons belonging to the equipotential layer $L$, which is at distance $r$ from the electrode centered on $C$, and $\Psi_i(t)$ is the given potential function of the $i$–$th$ neuron. In this study, the sensibility radius was set equal to 9 with a linear decaying function.

The EChG was recorded with a 6 channels virtual electrode system with one channel per *Ubidule* during 350 trials. Each trial had a fixed duration and included two intervals: a stimulation interval followed by an interstimulus interval. The stimulation was generated by spatio-temporal external stimuli applied only to the input layer of *o1Sensory* lasting 128 (*Type A*), 256, and 512 (*Type B*) time steps. The extensive use of Fast Fourier Transform in our signal analysis imposed, for improved efficiency, sampling frequencies which are powers of two. In practice the time-steps of the simulator were selected for convenient time units, *i.e.*, 1024 *time steps* corresponding to 1000 *ms*. The inter-stimulus interval was always equal to 1000 *ms*. The background activity to each neuron was set to 900 *spikes/s* with a low amplitude (1 *mV*) generated by uncorrelated Poisson distributed inputs. The recording time was divided into four periods defined following the amount of time the *Ubinet* was exposed to the stimulation: *(i) pre-learning* beginning at time zero and lasting 27 trials characterized by the absence of any stimulation (*i.e.*, only the background activity was present during the stimulation interval); *(ii) early-learning* lasting 50 trials, between trials #28 and #77; *(iii) late-learning* lasting 50 trials, between trials #228 and #277; and
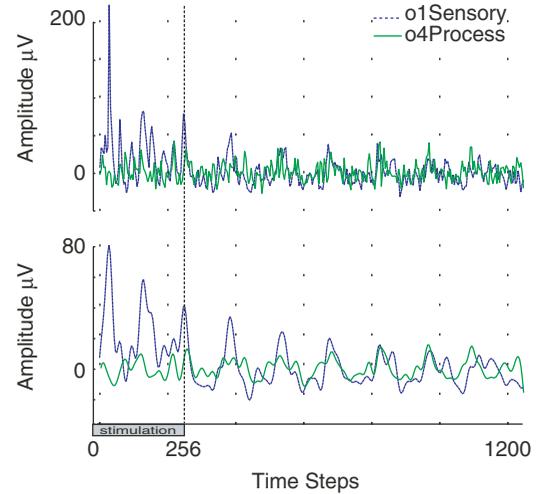


Fig. 5. Evoked potentials averaged over 50 trials obtained from *o1Sensory* (blue solid trace) and from *o4Process* (green dotted trace) *Ubidules* during the early-learning stage. The stimulus was applied during 256 time steps. The upper panel displays the raw evoked potentials and the lower panel shows the signals smoothed by a Blackmann smoothing window in order to emphasize the low frequency components.

*(iv) post-learning* lasting 50 trials, between trials #278 and #327.

The signals recorded *during the stimulation interval* were averaged across several trials in order to compute evoked potentials (*e.g.*, Fig. 5). The signals recorded *during the inter-stimulus interval* were used for bispectrum and bicoherence analyses. Let us consider the distribution of all phase-coupled frequencies $f_3$ observed in single-channel and cross-channel analyses. Let us consider the frequency band [1-24] *Hz* for EChG and *LF* the relative number of $f_3$ falling into this low frequency range. Let us consider the frequency band [60-84] *Hz* and *HF* the relative number of $f_3$ falling into this high frequency range. The *index of resonant frequencies IRF* is defined in the range 0–100 as follows: $IRF = \frac{1}{2} \times (100 + (\frac{HF - LF}{HF + LF} \times 100))$. This means a value of *IRF* close to 100 corresponds to a shift of $f_3$ towards higher frequencies and value of *IRF* close to 0 corresponds to a shift of $f_3$ towards lower frequencies. *IRF* values close to 50 indicates the phase-coupling was equally distributed in low- and high-frequency bands. Another index *RFR* – raw frequency ratio– is simply defined by $RFR = \frac{LF}{HF}$. This means a large value of *RFR* corresponds to a shift of phase-coupling towards higher frequencies and a low value of *RFR* corresponds to a shift towards lower frequencies.

## Human Recordings

All human Subjects were analyzed following a

protocol approved by the Ethical Committee of the Cantonal University Hospitals of Geneva (HCUGE). The data were anonymized before the analysis and no investigator was whatsover informed of any personal data of the Subjects. We have targeted a set of EEG recordings characterized by a non invasive treatment based on cognitive behavioural therapy (CBT-I) of insomnia (12, 32). Insomnia occurs in about a third of the adult population affecting both genders at all ages and observed in all countries, cultures, and races. This means that EEG changes associated to insomnia must reflect some very general pattern of alteration. The rationale is that such data set is keen to be similar to what we could explore along the "learning" procedure used with the *Ubinet*.

The subjective and polysomnographic improvement of sleep by CBT-I suggests that non-pharmacological treatments can induce significant changes in the EEG and that these changes might be associated to the dynamics of neural circuits that are involved in the etiology of insomnia. The hypothesis of a "hyperarousal" mechanism either physiologic, psychologic or cognitive has been suggested (37) and supported, among other findings, by electrophysiological markers. These markers include increased high EEG frequencies in the perisleep onset period, during non rapid eye movement (NREM) and rapid eye movement (REM) sleep (15, 26), reduction of slow wave sleep (16) and decreased of power spectra of *delta* 0.5-3.75 *Hz* and *theta* 3.75-6.75 *Hz* bands (29, 36). It appears that it is rationale to analyze the EEG from human Subjects and process it in the same way as the EChG from *Ubinet* in order to investigate common patterns of transition and alteration associated to the underlying network dynamics.

The polysomnography was performed on two patients and two control Subjects using 7 scalp silver-silver chloride EEG electrodes (*F*3-*F*4, *C*3-*C*4, *Cz*, *O*1-*O*2) referred to linked mastoid electrodes. Impedance was kept below 5 *k*Ω. In addition, two electrodes were placed above and below the external canthi for EOG, and two electrodes on the chin for EMG. The EEG recording was performed with a commercial device (Brainlab, OSG, Belgium) during the period 10 *PM*-8 *AM*. During wakefulness, at the beginning of the recording period, EEG epochs of interest were recorded during the *eyes closed* (EC) condition. The sleep onset was defined by the first disappearance of the *alpha* rhythm on all derivations and the appearance of a diffuse *theta* rhythm visible for more than 2 *sec*. The drowsiness period that occurred just before sleep onset is defined *post-hoc* at the time of the off-line analysis and corresponds to the *pre-theta* (PRE-THETA) recording condition. Changes in EEG spectral analysis in primary insomnia is most pro-eminent during the *first* ultradian sleep cycle. Then two minutes of EEG without artefacts
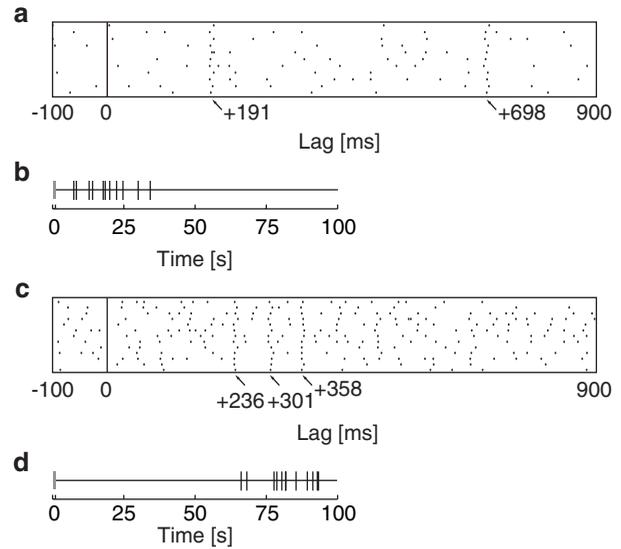


Fig. 6. Spatiotemporal firing pattern < 148*C*, 148*C*, 148*C*; 191 ± 0.9, 698 ± 1.0 > that repeated 11 times in the absence of apoptosis. Unit #148C spontaneous mean firing rate: 4.0 spikes/s. Raster plot **(a)** of the patterns aligned on the pattern start and raster plot of patterns onset **(b)**: each vertical tick corresponds to the onset time of each pattern occurrence; Spatiotemporal firing pattern < 554, 554, 554, 554; 236 ± 0.7, 301 ± 0.8, 358 ± 0.6 > in the absence of apoptosis. Unit #554 spontaneous mean firing rate: 13.1 spikes/s. Raster plot **(c)** showing 13 repetitions and raster plot of pattern onset **(d)**.

were collected for EC, PRE-THETA and first sleep cycle (NREM2, REM). In the human recordings the index of resonance *IRF* was calculated with *LF* [1-13] *Hz* and *HF* [33-48] *Hz* ranges.

## Results

### Preferred Firing Sequences

Precise firing sequences (PFS) are simply referred below as "patterns". Because of a high sensitivity to the initial conditions we repeated all simulation runs with 30 different random generator seeds.

Appearance and disappearance of patterns was due to developmental changes shaped by STDP in the network connectivity underlying the processing of temporal information. Fig. 6 shows extreme cases of onset dynamics of single-unit patterns observed in the absence of apoptosis. In one case a triplet appeared early in the network maturation and disappeared after $t \approx 35,000$ *ms* (Fig. 6, a and b). The single-unit pattern <148C, 148C, 148C; 191 ± 0.9, 698 ± 1.0> was composed by spikes produced by unit #148C. This notation means that a precise firing sequence started with a spike of unit #148C, followed 191 ± 0.9 milliseconds later by a second spike of the same unit, and followed by a third spike 698 ± 1.0 *ms* after the first. In the

**Table 1.  Cumulative statistics of preferred firing sequences detected in the downstream network**

|                       | stim OFF      | stim ON       | coupled 1     | coupled 2     |
|-----------------------|---------------|---------------|---------------|---------------|
| *Active neurons*      | 5352          | 4240          | 4860          | 3763          |
| *Detected Patterns*   | 197 (3.7%)    | 147 (3.5%)    | 241 (5%)      | 168 (5%)      |
| *Pattern Occurences*  | 7359 (38.5)   | 5672 (37.4)   | 9373 (39.9)   | 7853 (46.8)   |
| *Triplets/Quadruplets*| 59/138 = 0.4  | 54/93 = 0.6   | 107/134 = 0.8 | 89/99 = 0.9   |
| *Multi-unit Patterns* | 6             | 5             | 8             | 12            |

opposite case another pattern (a quadruplet in this example) appeared only at a later stage of maturation after $t \approx 65,000$ *ms* (Fig. 6c,d).

Table 1 shows cumulated statistics referred to the downstream network over all 30 simulation runs. This Table shows that in absence of an external input ('stim OFF')more units survive at the end of the simulation run.  In case of networks coupling more patterns were found in proportion to the number of active cells.  Moreover, in coupled networks each pattern tended to appear more often.  It is important to notice that both 'stim ON' and 'coupled 2' networks were characterized by 800 external afferent inputs. Despite this similarity there is a decrease in about 10% of the amount of surviving cells in the 'coupled 2' network by the end of simulation.  The ratio of detected patterns *vs*. active cells was close to 5% in the downstream network and $< 4\%$ in the upstream network (Table 1, second line).  This difference seems small overall but it was significant by $\chi^2$-test ($p < 0.05$).  The PGA algorithm detected all repetitions of the same pattern in the spike trains.  Notice that the average number of repetitions per pattern increased in the downstream network (up to 46.8 in 'coupled 2').

In all recording conditions we observed more patterns formed by four spikes (quadruplets) than patterns formed by three spikes (triplets).  However, the *Triplets/Quadruplets* ratio tended to values close to 1 in coupled networks (Table 1).  One could expect that most triplets corresponding to subpatterns of a significant quadruplet would also be counted among the significant triplets.  This is generally not the case because of the very stringent tests of significance carried on triplets that bias the pattern detection in the sense of underestimating the number of triplets (44). Most patterns were single-unit patterns but generally the units that were involved were different from pattern to pattern.  Depending on the recording condition we observed only 1-3 units that produced more than one single-unit pattern.  Multi-unit patterns were observed in all networks and they were more frequent in the 'coupled 2' downstream networks.  The probability of multi-unit pattern detection is very small due to the PGA sampling procedure for selection of the spike trains to be analyzed simultaneously.  Then,

the increase in frequency of multi-unit patterns could not be assessed with reliable confidence.

The analysis of the distribution of the intervals between the events forming the PFS was further investigated for the triplets by separating the "first intervals" (*i.e.*, between the first and second events of the patterns) and the "second intervals" (*i.e.*, between the second and third events of the patterns).  In case of quadruplets we considered the triplets corresponding to the subpatterns.  First intervals shorter than 100 *ms* were less frequent in the downstream networks compared to the first intervals of the upstream networks irrespective of the presence of the external stimulation.  Moreover, we found more patterns lasting between 100 and 400 *ms* in the downstream networks, thus suggesting a first order statistics that significantly deviated from Poisson distribution and an internal temporal structure that is associated with an increase in hierarchy of the *Ubidule*.

Fig. 7 shows the distribution of the onset time of the first occurrence of each pattern.  In all recording conditions most patterns appeared before $t = 30.000$ *ms* and not later than $t = 50.000$ *ms*.  In the downstream network (in particular 'coupled 2') the patterns tended to appear later during the simulation. Fig. 8 shows the distribution of the epochs of all spikes belonging to all repeated patterns.  It is interesting to notice that after a certain delay the probability to find a spike belonging to a pattern tended to be almost constant for all recording conditions.  However, such *plateau* was reached much later for the most interconnected downstream network (Fig. 8 'coupled 2'), at a time near $t = 35.000$ *ms*.

*Quadratic Phase Coupling*

The bispectral analysis was performed for all channels separatedly and the values of phase-coupled frequencies (*i.e.*, the frequencies of resonance $f_3$) were determined.

Fig. 9 shows the distribution of $f_3$ in the range 1 to 100 *Hz* during all recording periods and for the two types of stimulus used in the *Ubinet* simulation. These histograms show a shift towards an increase in lowfrequencies resonances during the *late-learning*
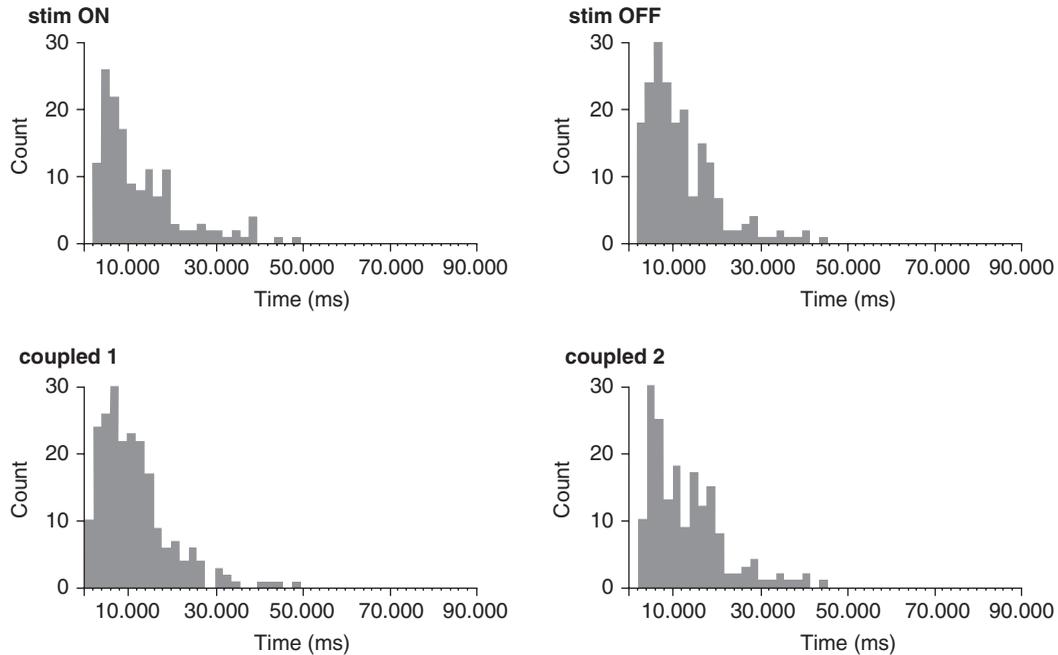
Fig. 7. Histogram of the onset time of all patterns. Bin size: 2000 *ms*. Notice the shift of the distribution towards later times for 'coupled 1' and 'coupled 2' networks, but in all cases the patterns appeared before time $t = 50.000$ *ms*.
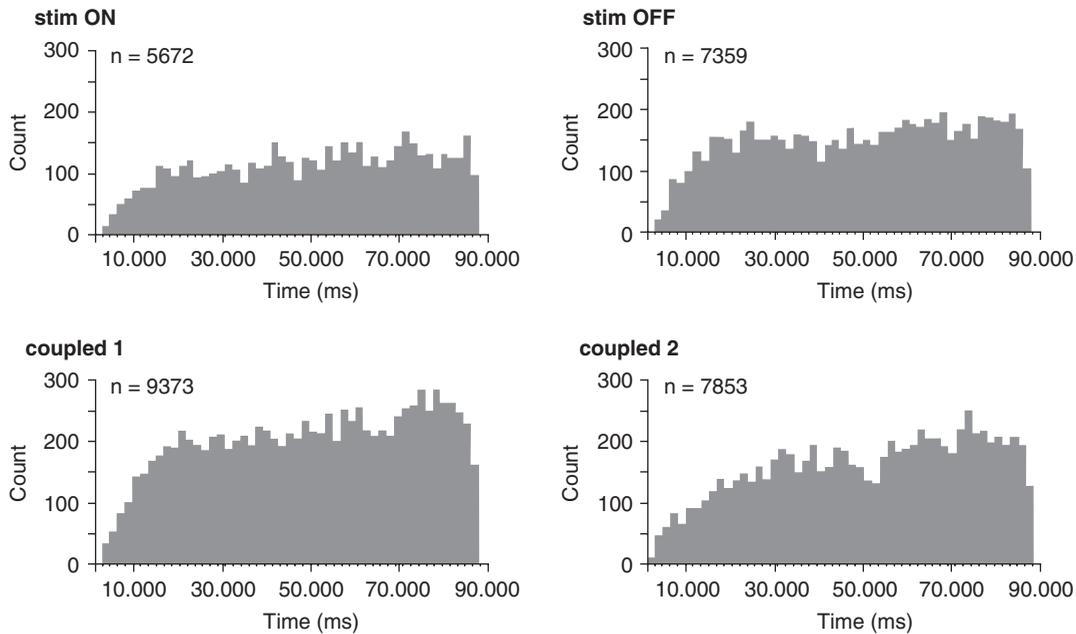


Fig. 8. Distribution of the epochs of all events belonging to all patterns. Bin size: 2000 *ms*. Notice the less steep slope for the 'coupled 2' downstream network.

phase, especially when compared with the distribution during the *post-learning*, when the input stimulus was absent. The quantitative assessment of this analysis presented in Table 2 emphasizes the change in the value of IRF between *early-* and *late-learning* phases. A decrease from $IRF \approx 60$ to values $IRF \approx 14$ followed by an increase to the range 26–29 during the *post-*learning phase suggests that the shift towards low frequencies of phase-coupling was provoked by the learning protocol and not only due to the maturation of the network. The analysis of *IRF* and *RFR* shows also that in the *postlearning* stage the resonant features remained affected by the functional connectivity that developed during the trials with external stimulation
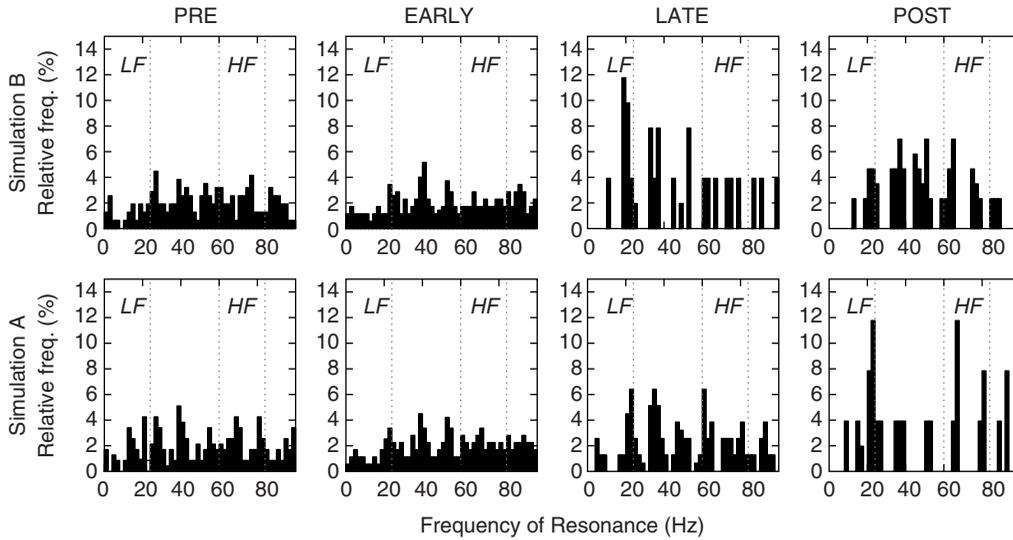
Fig. 9.  Relative distribution of the frequencies of resonance for each development period for Simulation A and B.  Bin size corresponds to 2 Hz intervals.  The dotted lines delineate the limits of *LF* and *HF* bands.

**Table 2.  Percentage of phase-coupled frequencies in each frequency bands of interest for the stimulus Type A and B within neural network development stages**

| Learning Phase | Percentage of phase-coupled frequencies | | | Indexes | |
|---|---|---|---|---|---|
| | LF: [1-24] *Hz* | [24-60] *Hz* | HF: [60-84] *Hz* | *IRF* | *RFR* |
| *Stimulus Type A* | | | | | |
| PRE | 281 | 545 | 210 | 43 | 1.34 |
| EARLY | 295 | 745 | 450 | 60 | 0.66 |
| LATE | 300 | 435 | 45 | 13 | 6.67 |
| POST | 85 | 110 | 30 | 26 | 2.83 |
| *Stimulus Type B* | | | | | |
| PRE | 265 | 635 | 430 | 62 | 0.62 |
| EARLY | 305 | 680 | 450 | 60 | 0.68 |
| LATE | 120 | 105 | 20 | 14 | 6.00 |
| POST | 170 | 150 | 70 | 29 | 2.43 |

*IRF*: index of resonant frequencies.  *RFR*: raw frequency ratio.

and the values were intermediate between *pre/early-learning* and *late-learning* phase.

Fig. 10 shows the distributions of phase-coupled frequencies in the range 1-50 *Hz* for all recording periods in controls and patients. A general observation is that for all Subjects and during all conditions the majority of phase-coupled frequencies were in the range 13-33 *Hz*. In addition, the histograms of Fig. 10 show that for patients before CBT-I treatment the relative count of phase-coupled frequencies in the range 33-48 *Hz* was larger than the count of phase-coupling in the low frequency range, up to 13 *Hz*. Notice that phase-coupled frequencies $f_3$ should not be confounded with the usual frequency bands of the EEG power spectra.

Table 3 shows the relative count of phase-

coupling in the frequency bands of interest and the values of indexes *IRF* and *RFR*. The general pattern was an increase of high frequency coupling in the group of patients before treatment. Then the main effect of treatment was to reduce high-frequency coupling and shift phasecoupling towards low frequencies, somehow with a significant increase of low frequency coupling compared to the controls. The effect of CBT-I treatment was tested against the control groups using $\chi^2 test$, $2P < 0.05$. In the *LF* range the patients before treatment show fewer phase-coupling than controls during all recording periods, but REM sleep (Table 3). The CBT-I treatment significantly increased the phase-coupling in the *LF* band during all other intervals, either re-establishing a level close to the controls or even beyond that level,

**Table 3. Percentage of phase-coupled frequencies in each frequency bands of interest for the the control group and for the group of patients before and after CBT-I treatment**

| Subject Group | Percentage of phase-coupled frequencies | | | Indexes | |
| --- | --- | --- | --- | --- | --- |
| | LF: [1-13] *Hz* | [13-33] *Hz* | HF: [33-48] *Hz* | *IRF* | *RFR* |
| *Eyes Closed* | | | | | |
| Control | 12 | 74 | 14 | 54 | 1.17 |
| Patient before | 2 (*) | 77 (ns) | 21 (ns) | 91 (*) | 10.50 |
| after CBT-I | 8 (ns) | 88 (ns) | 4 (*) | 33 (ns) | 0.50 |
| *Pre-Theta* | | | | | |
| Control | 12 | 5 | 13 | 52 | 1.08 |
| Patient before | 3 (*) | 87 (ns) | 10 (ns) | 77 (ns) | 3.33 |
| after CBT-I | 3 (*) | 96 (ns) | 1 (**) | 25 (*) | 0.33 |
| *NREM* | | | | | |
| Control | 57 | 30 | 13 | 19 | 0.23 |
| Patient before | 27 (*) | 60 (*) | 13 (ns) | 33 (*) | 0.48 |
| after CBT-I | 42 (ns) | 57 (*) | 1 (**) | 2 (*) | 0.02 |
| *REM* | | | | | |
| Control | 4 | 90 | 5 | 56 | 1.25 |
| Patient before | 4 (ns) | 85 (ns) | 12 (ns) | 75 (ns) | 3.00 |
| after CBT-I | 19 (*) | 79 (ns) | 2 (ns) | 10 (*) | 0.11 |

*IRF*: index of resonant frequencies.  *RFR*: raw frequency ratio.
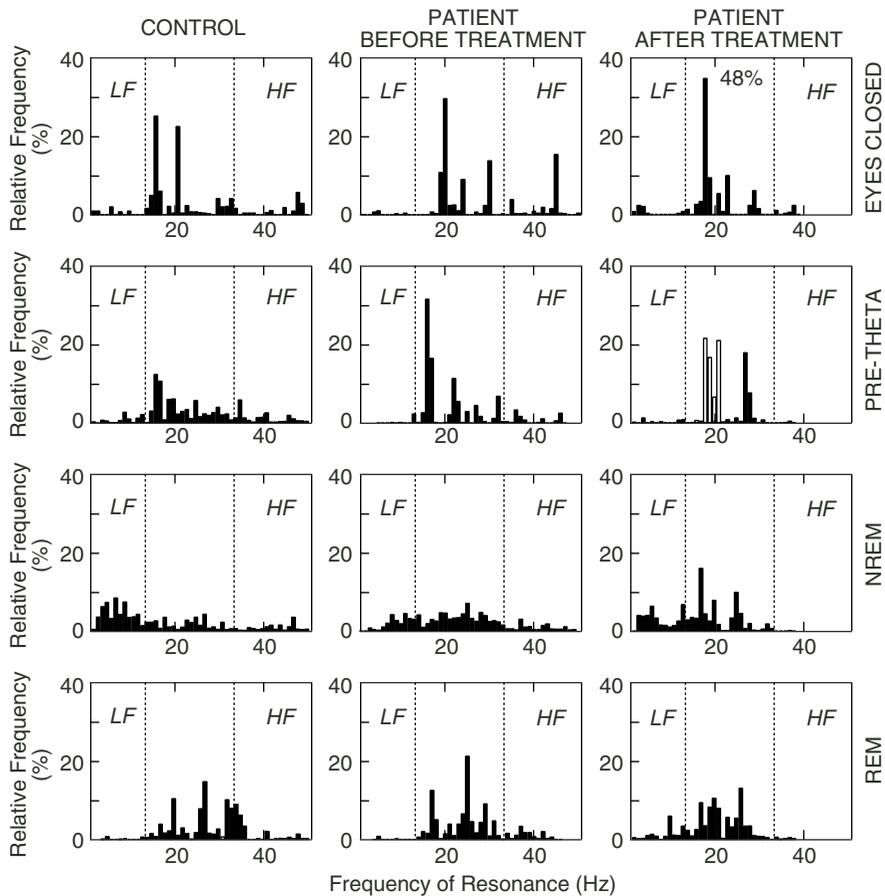Significance levels: (ns) not significant, (*) 5%, (**) 1%.



Fig. 10.  Relative distribution of the frequencies of resonance for control and patient groups before and after CBT-I treatment.  Bin size corresponds to 1 Hz intervals.  The dotted lines delineate the limits of *LF* and *HF* bands.

as observed during REM. The mid-range (13-33 *Hz*) phase-coupling was not affected by the CBT-I treatment. In the *HF* range the treatment significantly reduced the phase-coupling by a shift towards lower frequencies during all recording periods, but REM.

## Discussion

This paper described the implementation of a neuronal system simulator on a hybrid scalable multi-agent hardware platform based on the *Ubidules* framework (41) and its application to the study of information processing in hierarchically organized neural networks circuits. In coupled *Ubidules* we recorded the spike trains of all neurons and the usual neurophysiological analyses could be applied to assess the effect of hierarchical projections. We have explored one simple *Ubinet* network circuit characterized by a sensory network processing the external input that projects to a hierarchically organized multilayered (in our case formed by only two layers) network of processing areas which eventually project on a motor network that generates an activity keen to be encoded into actuators. The *Ubinet* activity was studied by virtual electrodes that recorded neural signals –electrochipograms (EChG)– comparable to EEG and that could be analyzed using the same techniques, in particular third order cumulant analysis (7, 11).

In paired networks we recorded the spike trains of all excitatory units that were not directly stimulated and that were surviving at the arbitrary end of simulation runs set at $t = 100.000$ time steps. The results show that the downstream network activity was characterized by fewer surviving cells at the end of the simulation run. This difference was only due to synaptic pruning driven by STDP because cell death provoked by apoptosis was similar for both upstream and downstream networks. We searched for spatiotemporal firing patterns (PFS) in detail using the PGA technique (44, 45). In presence of an external stimulus PFS observed in the upstream network were relatively more frequent than in the absence of stimulation, thus confirming our previous results (22). Despite the number of active cells was smaller the number of patterns was larger in the downstream network.

The analysis of the onset time of the patterns and their internal dynamics suggests that downstream networks took more time to build-up the connectivity underlying the emergence of the patterns. This tendency was enhanced in case of divergent and stronger connectivity towards the downstream network ('coupled 2' condition). The finding of what could be viewed as an increase in "complexity" of the temporally organized activity in the upstream network is achieved with less active units and in a totally un-

supervised way. This observation is in agreement with experimental observations of a general pattern of axonal and synaptic pruning during neural development (25, 28). We may suggest that the outcome of this process could be the emergence of a hierarchical connectivity better suited to process temporal information, also in agreement with gradient-like organization observed during early corticogenesis (13).

The experimental approach to the *Ubinet* activity by recording the EChG was aimed to assess the effect of a repeated stimulation on the functional connectivity established between the *Ubidules*. Our pre-learning stage could represent a control situation driven exclusively by the background activity of the subject's brain. The subject is naive to the coming stimulus so that a learning process can occur. During the early-learning stage the repetition of the stimuli at regular intervals may initiate a recognition process that will eventually shape the functional connectivity of feature detecting cell assemblies after selective synaptic and cell pruning.

The third order spectral analysis of EChG and EEG allows to determine the frequency range of quadratic phase coupling (resonant frequency) across cortical areas (49, 50). According to the usual interpretation based on standing waves theory, high resonant frequencies mean that information processing is transmitted at short distance (*i.e.*, the distance between two nodes of the wave). A coupling that occurs at high frequencies may be interpreted as a sign of focal cortical interactions. Conversely, a coupling at low frequencies suggests an increased cross-areal involvement in neural processing.

A remarkable result is the finding that late-learning stages in the *Ubinet* simulations were characterized by a value of *IRF* ≈ 14 compared with pre- and early-learning stages (*IRF* in the range 43-62). In the study with human Subjects we observed that controls and patients after CBT-I treatment were characterized, during all sleep phases by values of *IRF* lower than insomniac patients before treatment. It is also worth reporting that the only condition that let appear a difference of resonant frequencies in the range [13-33] *Hz* was during NREM sleep irrespective of the treatment. This last result suggests that despite an overall shift of resonant frequencies towards recovery, focal cortical interactions tended to persist in patients during non-REM (NREM) sleep periods. This is in agreement with the finding of decreased regional cerebral blood flow during NREM reported in the subcortical, limbic/arousal systems and in the anterior cingulate and medial prefrontal areas of patients compared to normal controls (33).

The comparison between the *Ubidules* and human recordings suggests that *Ubinet* activity during the pre and early-learning stages is characterized by

features similar to the insomniac brain, with too many high resonant frequencies. Then, an appropriate stimulation of the *Ubinet* as well as cognitive brain therapy are both modifying the ratio of resonant frequencies provoking a shift of the indexes towards low frequencies at all brain states. The prevalence of high frequencies of resonance in chronic primary insomniac patients may be associated to the prevalence of multiple sites of focal cortical interactions, which supports the "hyperarousal" hypothesis in insomniac patients (5, 37). However, what is the meaning of "hyperarousal" in an artificial brain? Moreover, the question whether robots need to sleep (14) has been raised.

Our findings suggest that new tools provided by modular and scalable neural network simulators offer new opportunities to neurophysiologists and clinicians to test hypotheses based on the analysis of neural signals, at the microscopic level with spike trains and at mesoscopic levels with EChG. The future work is also aimed to test other neural circuits and other neuronal models to provide a fully fledged testable platform based on numerous interacting and evolvable neural application agents suitable for implementation on mobile robots.

## Acknowledgments

## References

1. Abeles, M. *Corticonics: Nzural Circuits of the Cerebral Cortex.* Cambridge: University Press, 1991.
2. Ashikaga, M., Kikuchi, M., Hiraguchi, T., Sakura, M., Aonuma, H. and Ota, J. Foraging task of multiple mobile robots in a dynamic environment using adaptive behavior in crickets. *J. Robotics Mech.* 19: 466-473, 2007.
3. Bellifemine, F.L., Caire, G. and Greenwood, D. *Developing Multi-Agent Systems With JADE.* Hoboken, N.J.: Wiley, 2007.
4. Benoskova, L. and Kasabov, N. *Computational Neurogenetic Modeling.* Spriger, New York, NY, USA, 2007.
5. Bonnet, M.H. and Arand, D.L. Hyperarousal and insomnia. *Sleep Med. Rev.* 1: 97-108, 1997.
6. Braitenberg, V. and Schuez, A. *Cortex: statistics and geometry of neuronal connectivity.* Springer, Berlin, second edition, 1998.
7. Brillinger, D.R. An introduction to polyspectra. *Ann. Math. Stat.* 36: 1351-1374, 1965.
8. Chechik, G., Meilijson, I. and Ruppin, E. Neuronal regulation: A mechanism for synaptic pruning during brain maturation. *Neural Comput.* 11: 2061-2080, 1999.
9. Conel, J.L. *The Post Natal Development of the Human Cerebral Cortex, 6 Vols.* Cambridge, MA: Harvard University Press, 1939-1963.
10. Doya, K. and Uchibe, E. The cyber rodent project: Exploration of adaptive mechanisms for self-preservation and self-reproduction. *Adapt. Behav.* 13: 149-160, 2005.
11. Dumermuth, G., Huber, P.J., Kleiner, B. and Gasser, T. Analysis of the interrelations between frequency bands of the EEG by means of the bispectrum. a preliminary study. *Electroencephalogr. Clin. Neurophysiol.* 31: 137-148, 1971.
12. Edinger, J.D. and Means, M.K. Cognitiveñbehavioral therapy for primary insomnia. *Clin. Psychol. Rev.* 25: 539-558, 2005.
13. Elston, G.N. Cortical heterogeneity: implications for visual processing and polysensory integration. *J. Neurocytol.* 31: 317-335, 2002.
14. Fouks, J.D., Besnard, S., Signac, L., Meurice, J.C., Neau, J.P. and Paquereau, J. Do robots need to sleep? *Neurophysiologie Clinique,* 34: 59-70, 2004.
15. Freedman, R. EEG power speactra in sleep-onset insomnia. *Electroencephalograph Clin. Neurophysiol.* 63: 408-413, 1986.
16. Gaillard, J.M. Chronic primary insomnia: possible physio-pathological involvement of slow wave deficiency. *Sleep* 1: 133-147, 1978.
17. Hill, S. and Villa, A.E. Dynamic transitions in global network activity influenced by the balance of excitation and inhibtion. *Network-Comp. Neural.* 8: 165-184, 1997.
18. Hubel, D.H., Wiesel, T.N. and LeVay, S. Plasticity of ocular dominance columns in monkey striate cortex. *Philos. Trans. R. Soc. Lond. B. Biol. Sci.* 278: 377-409, 1977.
19. Huttenlocher, P.R. Synaptic density in human frontal cortex – Developmental changes and effects of aging. *Brain Res.* 163: 195-205, 1979.
20. Iglesias, J., Chibirova, O. and Villa, A. Nonlinear dynamics emerging in large scale neural networks with ontogenetic and epigenetic processes. *Lect. Notes Comput. Sci.* 4668: 579-588, 2007.
21. Iglesias, J., Eriksson, J., Grize, F., Tomassini, M. and Villa, A.E. Dynamics of pruning in simulated large-scale spiking neural networks. *BioSystems* 79: 11-20, 2005.
22. Iglesias, J. and Villa, A.E.P. Effect of stimulus-driven pruning on the detection of spatiotemporal patterns of activity in large neural networks. *BioSystems* 89: 287-293, 2007.
23. Iglesias, J. and Villa, A.E.P. Emergence of preferred firing sequences in large spiking neural networks during simulated neuronal development. *Int. J. Neural Syst.* 18: 267-277, 2008.
24. Innocenti, G.M. Exuberant development of connections, and its possible permissive role in cortical evolution. *Trends Neurosci.* 18: 397-402, 1995.
25. Innocenti, G.M. and Price, D.J. Exuberance in the development of cortical networks. *Nat. Rev. Neurosci.* 6: 955-965, 2005.
26. Lamarche, C.H. and Ogilvie, R.D. Electrophysiological changes during the sleep onset period of psychophysiological insomniacs, psychiatric insomnias, and normal sleepers. *Sleep* 20: 724-733, 1997.
27. Levitt, P. Structural and functional maturation of the developing primate brain. *J. Pediatr.* 143: S35-S45, 2003.
28. Low, L.K. and Cheng, H.-J. Axon pruning: an essential step underlying the developmental plasticity of neuronal connections. *Philos. T. Roy. Soc.* 361: 1531-1544, 2006.
29. Merica, H., Blois, R. and Gaillard, J.M. Spectral characteristics of sleep EEG in chronic insomnia. *Eur. J. Neurosci.* 10: 1826-1834, 1998.
30. Mizuno, H., Hirano, T. and Tagawa, Y. Evidence for activity-dependent cortical wiring: formation of interhemispheric connections in neonatal mouse visual cortex requires projection neuron activity. *J. Neurosci.* 27: 6760-6770, 2007.
31. Montgomery, J.M. and Madison, D.V. Discrete synaptic states define a major mechanism of synapse plasticity. *Trends Neurosci.* 27: 744-750, 2004.
32. Morin, C.M., Vallières, A., Guay, B., Ivers, H., Savard, J., Mérette, C., Bastien, C. and Baillargeon, L. Cognitive behavioral therapy, singly and combined with medication, for persistent insomnia. *J. Am. Med. Assoc.* 301: 2005-2015, 2009.
33. Nofzinger, E.A., Buysse, D.J., Germain, A., Price, J.C., Miewald, J.M. and Kupfer, D.J. Functional neuroimaging evidence for hyperarousal in insomnia. *Am. J. Psychiat.* 161: 2126-2129, 2004.

34. Nunez, P.L. and Srinivasan, R. *Electric Fields of the Brain.* Oxford University Press, 2006.

35. Oppenheim, R.W. Studies in developmental neurobiology: Essays in honor of Viktor Hamburger. In Cowan, W.M., editor, *The neurotrophic theory and naturally occurring motoneuron death.* Oxford University Press, 1981.

36. Perlis, M.L., Smith, M.T., Orff, H., Andrews, P. and Giles, D.E. Beta/gamma activity in patients with insomnia and in good sleeper controls. *Sleep* 24: 110-117, 2001.

37. Perlis, M.L., Smith, M.T. and Pigeon, W.R. Etiology and pathophysiology of insomnia. In: *Principles and Practice of Sleep Medicine*, edited by Kryger, M., Roth, T., and Dement, W.C. Philadelphia, PA: Elsevier Saunders, pp. 726-737, 2005.

38. Press, W.H., Flannery, B.P., Teukolsky, S.A. and Vetterling, W.T. *Numerical recipes in C: The art of scientific computing.* Cambridge, England: Cambridge University Press, 1992.

39. Ramakers, G.J. Neuronal network formation in human cerebral cortex. *Prog. Brain Res.* 147: 1-14, 2005.

40. Roberts, P.D. and Bell, C.C. Spike timing dependent synaptic plasticity in biological systems. *Biol. Cybern.* 87: 392-403, 2002.

41. Sanchez, E., Perez-Uribe, A., Upegui, A., Thoma, Y., Moreno, J.M., Villa, A., Volken, H., Napieralski, A., Sassatelli, G. and Lavarec, E. Perplexus: pervasive computing framework for modeling complex virtually-unbounded systems. In *AHS '07: Proceedings of the Second NASA/ESA Conference on Adaptive Hardware and Systems*, pages 587-591,Washington, DC, USA, 2007. IEEE Computer Society.

42. Shaposhnyk, V.V., Dutoit, P., Contreras-Lámus, V., Perrig, S. and Villa, A.E.P. A framework for simulation and analysis of dynamically organized distributed neural networks. *Lect. Notes Comput.*

43. Shatz, C.J. Impulse activity and the patterning of connections during cns development. *Neuron* 5: 745-756, 1990.

44. Tetko, I.V. and Villa, A.E. A pattern grouping algorithm for analysis of spatiotemporal patterns in neuronal spike trains. 1. detection of repeated patterns. *J. Neurosci. Meth.* 105: 1-14, 2001.

45. Tetko, I.V. and Villa, A.E. A pattern grouping algorithm for analysis of spatiotemporal patterns in neuronal spike trains. 2. application to simultaneous single unit recordings. *J. Neurosci. Meth.* 105: 15-24, 2001.

46. Torres, O., Eriksson, J., Moreno, J.M. and Villa, A.E. Hardware optimization and serial implementation of a novel spiking neuron model for the poetic tissue. *BioSystems* 76: 201-208, 2004.

47. Villa, A. E., Tetko, I., Hyland, B. and Najem, A. Spatiotemporal activity patterns of rat cortical neurons predict responses in a conditioned task. *Proc. Natl. Acad. Sci. U.S.A.* 96: 1106-1111, 1999.

48. Villa, A.E.P. Empirical evidence about temporal structure in multi-unit recordings. In: *Time and the Brain*, edited by Miller, R. Chur, Switzerland: Harwood Academic Publishers, pp. 1-51, 2000.

49. Villa, A.E.P., Tetko, I.V., Dutoit, P., De Ribaupierre, Y. and De Ribaupierre, F. Corticofugal modulation of functional connectivity within the auditory thalamus of rat. *J. Neurosci. Meth.* 86: 161-178, 1999.

50. Villa, A.E.P., Tetko, I.V., Dutoit, P. and Vantini, G. Non-linear cortico-cortical interactions modulated by cholinergic afferences from the rat basal forebrain. *BioSystems*, 58: 219-228, 2000.

51. Yamamori, T. and Rockland, K.S. Neocortical areas, layers, connections, and gene expression. *Neurosci. Res.* 55: 11-27, 2006.

*Sci.* 5768: 277-286, 2009.